International Journal of Heat and Mass Transfer 52 (2009) 1385–1399

Contents lists available at ScienceDirect

International Journal of Heat and Mass Transfer

journal homepage: www.elsevier.com/locate/ijhmt

Heat transfer enhancement via liquid–liquid phase separation

S. Gat, N. Brauner, A. Ullmann *

Department of Fluid Mechanics and Heat Transfer, Faculty of Engineering, Tel Aviv University, Tel Aviv, Israel

ARTICLE INFO

Article history:
Received 14 January 2008
Received in revised form 20 August 2008
Available online 1 November 2008

Keywords:
Heat transfer
Convective
Free convection
Critical solution
Phase separation
Spinodal decomposition
Metastable decomposition

ABSTRACT

The heat transfer and flow phenomena during phase separation of partially miscible liquid solvent system were investigated experimentally. The experiments were conducted with a three components system which has an upper critical solution temperature, using critical and off-critical compositions of the solvent mixtures. The convective heat transfer rates were studied for laminar flow in a small diameter horizontal tube and for free convection from its outer surface. It was found that with phase separation the forced convective heat transfer can be augmented by up to 130% compared to heat transfer rates obtained in single phase flow (without phase separation). However, for low quenching rate and depth associated mainly with experiments conducted with critical compositions, deterioration of the heat transfer rates was observed. The free convection heat transfer coefficients were found to be augmented up to 100%. Macro- and micro-flow visualization were also conducted to follow the flow phenomena during the phase separation, and the mechanisms responsible to the heat transfer enhancement are discussed.

© 2008 Elsevier Ltd. All rights reserved.

1. Introduction

Boiling heat transfer is common in various industrial applications, including mini and microelectronic systems, which are characterized by high heat transfer rates. The high heat transfer rates during heterogeneous boiling are commonly attributed to the pumping mechanism due to the bubble detachment from the heated surface [1,2]. Bubble detachment results in inflow of fresh, cold liquid into the thermal boundary layer, thus increases the rate of heat removal from the surface. However, the heat transfer efficiency is deteriorated when the detaching bubble size is of the order of the channel diameter. In such cases, earlier dry out occurs, causing a significant drop in heat transfer rates, below the rates obtained in single phase liquid flows. Hence, using phase change mechanism for cooling is inefficient in small diameter channels, which are typical in cooling devices of mini-electronic systems [3–5].

To overcome the above limitations of boiling in small diameter pipes, while preserving the 'pumping effect', the possibility of using phase separation of liquid solutions, instead of evaporating systems, for enhancing heat transfer rates has been tested in this study. The liquid solutions used are partially miscible solvent systems, with a Critical Solution Temperature (CST). Such systems can alter from a state of a single liquid phase, to a state of two separated liquid phases, by a small change of temperature. In solvent systems that are characterized by an Upper Critical Solution Temperature (UCST), the transition from a single phase to two phases is brought about by reducing the temperature. In other solvent systems, which are characterized by lower CST (LCST), the phase separation occurs with increasing the temperature. A detailed list of a variety of binary and multi-component systems possessing a critical temperature was collected by Francis [6].

Thermodynamic equilibrium of solvent system is a well-known subject, which can be found in many textbooks [7,8]. A system of a well-defined composition will separate into two phases only if the Gibbs free energy, G, of the separated two phases is lower than that of the original mixture (Fig. 1a). This behavior characterizes only non-ideal solutions. The locus of the compositions of the separated phases in equilibrium is denoted as the coexistence (or binodal) curve (see Fig. 1b).

The spinodal curve (Fig. 1b) represents transition between meta-stable and unstable regions. The meta-stable region extends between the spinodal and binodal curves. A solution having composition in this region would be stable to small changes in temperature, pressure and concentration. However, a sufficiently large perturbation can lead to a spontaneous phase separation to two liquid phases with compositions determined by the coexistence curve (e.g. points a and h in Fig. 1a). The different regions of stability are sensitive to temperature changes (only slightly to pressure). Referring to the phase diagram shown in Fig. 1b, a maximum temperature at which phase change can occur exists, and is denoted as the Upper Critical Solution Temperature (UCST). In a three-component system, the equilibrium temperature–composition relations are more complicated [7,8]. The equilibrium data of the two coexisting phases can be represented by a 3-dimensional surface, reflecting the variation of temperature and the compositions of two of the components (see Appendix A). When the relation

* Corresponding author. Tel.: +972 36407829; fax: +972 36407334.
E-mail address: ullmann@eng.tau.ac.il (A. Ullmann).

0017-9310/$ - see front matter © 2008 Elsevier Ltd. All rights reserved.
doi:10.1016/j.ijheatmasstransfer.2008.08.020

Nomenclature

A	surface area [m^2]
AF	augmentation factor, Eq. (5)
C_p	specific heat [$J\,kg^{-1}\,°C^{-1}$]
D	tube inner diameter [m]
d	drop diameter [m]
G	Gibbs free energy [J]
G_{ij}	binary interaction parameter (calculated)
g	acceleration due to gravity [$m\,s^{-2}$]
h	heat transfer coefficient [$W\,m^{-2}\,°C^{-1}$]
H_{mix}	heat of mixing [$J\,kg^{-1}$]
k	thermal conductivity [$W\,m^{-1}\,°C^{-1}$]
L	length of the tube test section [m]
Nu_D	Nusselt number, dimensionless
Pe	Peclet number, UD/α, dimensionless
Pr	Prandtl number, dimensionless
Q	heat transfer rate [W]
R	universal gas constant [$J\,K^{-1}\,mol^{-1}$]
Ra_D	Rayleigh number, dimensionless
Re_D	Reynolds number, dimensionless
St_D	Stanton number, dimensionless
T	temperature [°C, K]
ΔT_{lm}	log-mean temperature difference [°C]
t	time [s]
U	fluid average velocity [$m\,s^{-1}$]
$\dot{V}$	volumetric flow rate [$m^3\,s^{-1}$]
v	lateral velocity [$m\,s^{-1}$]
x	mol fraction

Greek symbols

α	thermal diffusivity [$m^2\,s^{-1}$]
α_{ij}	interaction parameter (symmetric)
γ	activity coefficient
λ	binary interaction energy [$J\,mol^{-1}$]
μ	viscosity [$N\,s\,m^{-2}$]
ρ	density [$kg\,m^{-3}$]
σ	surface tension [$N\,m^{-1}$]
τ_{ij}	interaction parameter (asymmetric)

Subscripts

1, 2	phases index
b	bulk
cp	cloud point
f	film
i, j	phases index
sp	single phase
w	wall

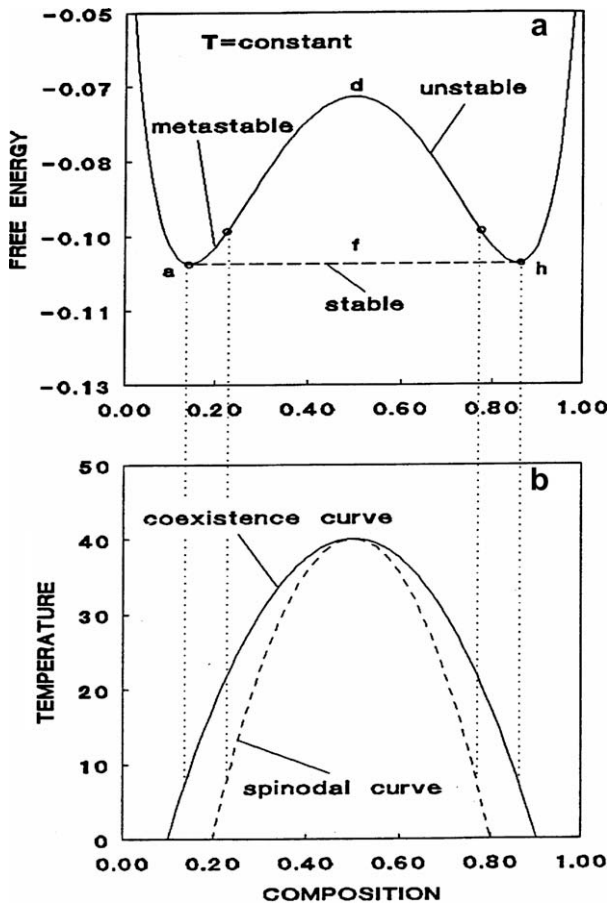

Fig. 1. (a) Gibbs energy of mixing for binary systems as a function of solvent system composition, (b) coexistence curve and spinodal curve.

between composition, temperature and Gibbs free energy is known, the critical temperature and the equilibrium compositions at various states can be estimated. To this aim, several well-known models/correlations for calculating the chemical potential (e.g. UNIQUAC, NRTL, Van Leer) can be found in the literature [7].

As previously stated, phase separation of CST mixtures can be induced by temperature change. In general, there are two types of phase separation: spinodal decomposition (SD) for systems that are in an unstable equilibrium state, and nucleation for systems in the meta-stable state. When an UCST mixture experiences a temperature quench, depending on the overall composition and the quench depth, three different cases are considered: with a mixture of a critical composition, any quench below the coexistence curve will lead to the unstable region, and therefore to SD; With solutions of off-critical compositions, a 'shallow' quench will results in meta-stable decomposition (nucleation), and a deep quench of off-critical compositions will lead the system to the unstable SD region.

The SD of critical composition mixture is characterized by the formation of non-localized concentration fluctuations, with no definite separating interfaces. These domains of different concentration grow rapidly, leading to fast phase separation [9]. Their size and concentration varies with time. The typical domain size is described by power law time dependence, t^n, where $n \sim 1/3$ is characteristic of a diffusion dominated process, while with $n \sim 1$ convection dominates. Moreover, due to the rapid separation, and in the absence of definite boundaries, the growth rate is not affected by presence of surfactants [10–14]. On the other hand, the meta-stable decomposition is characterized by nucleation and growth of droplets, and was found to be rather slow compared to the separation rate associated with SD [15,16]. With a deep quench of off-critical composition, the separation starts as a meta-stable decomposition, which is then followed by the SD. It is important to note, that the whole phase separation process is accelerated as the quench is deeper [17].

The SD is associated with isotropic convective motion, generated by non-equilibrium capillary forces, with a characteristic velocity between 0.1 and 1 mm/s [18]. Such a convective motion with droplet velocity of about 0.5 mm/s was also reported by Arce et al. [19]. At the final stage of the SD, the domain size becomes large and the convective motion and phase separation are dominated by gravity. The convective motion during the SD was shown to increase the heat transfer rates in a closed cell above those obtained by heat conduction [20].

Based on the phenomena associated with the phase separation, it can be postulated that the process can be beneficially used for enhancing convective heat transfer in flowing systems in comparison to single-phase flow. On the other hand, in comparison to vapor–liquid systems, partially miscible solvent systems are characterized by a very low surface tension and heat of solution. Thus, in comparison to vapor–liquid phase change, the heterogeneous separation of a CST mixture is expected to be characterized by a formation of smaller drops at higher rates for a given heat flux. In particular, due to the formation of small liquid droplets (rather then larger bubbles), the phase separation can be beneficially used for enhancing heat transfer rates in small diameter channels, where the dry out phenomenon limits the efficiency of boiling heat transfer.

Enhancement of heat transfer rates can also be expected in free convection. The later is generally driven by density difference. In pure component single-phase systems, or in solvent systems above the cloud point, the density difference is solely due to density–temperature variation. In this case, a small temperature gradient results in a small density difference, and hence, relatively low heat transfer rates. On the other hand, by using a CST solvent system, a higher density difference can be achieved for the same temperature driving force. Therefore, an improved free convection heat transfer coefficient may be expected.

This study is aimed at testing the feasibility of enhancing convective heat transfer rates, while maintaining a low temperature driving force, via liquid–liquid phase separation. The experimental work is concentrated on forced convection heat transfer in horizontal pipe flow. Additional test were conducted also on free convection heat transfer from surfaces.

2. Experimental setup and procedure

2.1. The solvent system

An 'upper CST' three-component solvent system, composed of water–ethanol–ethyl acetate (WEA) was used. This solvent system was selected as its components are non-toxic and can be safely used also in large volumes. Three basic systems, related to three different sets of tie-lines, were used. These correspond to sets of tie-line *a*, *b*, *c* in Fig. 2a, which possesses a maximal complete miscibility temperature (denoted by CST) of 50, 37 and 28 °C, respectively (Fig. 2b and c). With these solvent systems, experiments were conducted with critical and off-critical (organic-rich and water-rich) compositions (see Table 1a and Fig. 2). The variation of the cloud point temperature, T_{cp}, with composition for each of the three systems was obtained experimentally based on the equilibrium compositions calculated with the NRTL model at the lowest tested temperature (20 °C or 7 °C). The experimental procedure and the explanation of the way the equilibrium data is presented in Fig. 2 are given in Appendix A.

Note that, because of the relatively high volatility of the organic solvents and working temperatures above the ambient, the composition, and hence the cloud point of the solvent mixture varied during the experiments. Therefore, the mixture was routinely sampled during the experiment and its cloud point was monitored. When significant changes where detected, the composition was readjusted. The change of composition due to solvent evaporation was detected mainly in the free convection experiments, where the solvents were kept in unsealed container. Therefore, the free convection experiments were conducted mainly with water-rich compositions and at relatively low temperatures.

2.2. Experimental setup for forced convection heat transfer

The schematic description experimental setup is shown in Fig. 3. A 20-L glass tank of a 28-cm diameter is used as a heating/cooling environment. In the convective heat transfer experiments the tank contains cooled water. The tank is covered with a Teflon plate to minimize losses due to evaporation. The heating element, temperature controller, stirring rod and mixing baffles are mounted on this cover. The forced convection experiments were studied in a U-shaped stainless steel (3 1 6) tube with an outer diameter of D_o = 4 mm and an inner diameter of D = 2 mm. The vertical sections of the U tube are isolated, and the heat transfer is studied in the 16 cm length horizontal section of the tube.

A temperature controlled circulating bath is used for circulating the solvent through the tube. The temperature of the water in the tank, the inlet and outlet temperatures of the solvent mixture flowing in the tube and the tube surface temperature at eight locations are measured by T-type thermocouples (with accuracy of ±0.1 °C, which was achieved by a careful calibration). A stirrer is used to mix the water in the tank and thus to maintain a uniform temperature outside the pipe. The temperature was controlled by using both heating and cooling elements. The data acquisition system uses A/D card and the LabView software.

The CST mixture was heated in the circulating bath, where the temperature was controlled to the required operating temperature (above the cloud point). The temperature of water in the tank was kept at a constant and uniform temperature below the cloud point. In principle, three modes of operation are possible. In the first mode, the CST mixture enters the test section of the tube with temperature below the cloud point, resulting in two-phase flow of the separating phases throughout the test section. In the second mode, the CST mixture enters the test section above the cloud point and exits it below the cloud point temperature. If the wall temperature is above the cloud point, a third mode become possible, in which the CST mixture flows as a single phase throughout the test section. In all these three modes, the heat transfer rates were tested for different flow rates (measured with 5% accuracy). In all the experiments conducted, the flow in the pipe was laminar, with Reynolds number varying in the range of Re = 260–1100. The reported results correspond to steady state conditions, which were typically achieved after at least five liquid content replacements in the pipe.

The experimental convective heat transfer coefficients can be calculated using the following equations:

$$Q = \rho \cdot \dot{V} \cdot (\Delta H_{\text{sensible}} + \Delta H_{\text{mixing}})_{\text{CST mixture}}; \quad h = \frac{Q}{A_{\text{in}} \cdot \Delta T_{\text{lm}}} \tag{1.1}$$

$$\Delta H_{\text{sensible}} = C_p \cdot (T_{in} - T_{\text{out}}); \quad \Delta H_{\text{mixing}} = H_{\text{ex}}^{\text{in}} - H_{\text{ex}}^{\text{out}}; \tag{1.2}$$

where the density and the heat capacity of the solvent mixture, ρ and C_p, were calculated based on the overall composition and the average temperature, A_{in} is the internal surface area of the tube test section, T_{in} and T_{out} are the inlet and outlet temperatures of the solvent mixture, $\dot{V}$ is the volumetric flow rate and ΔT_{lm} is the log-mean temperature difference between the wall surface and the bulk of the flowing mixture. The enthalpy change due to mixing, ΔH_{mixing} is given by the difference between the excess enthalpy, H_{ex}, of the inlet and outlet streams, where H_{ex} is the difference between the enthalpy of the mixture and that of an ideal mixture. Unfortunately, reliable values of the heat of mixing for the WEA 3-component

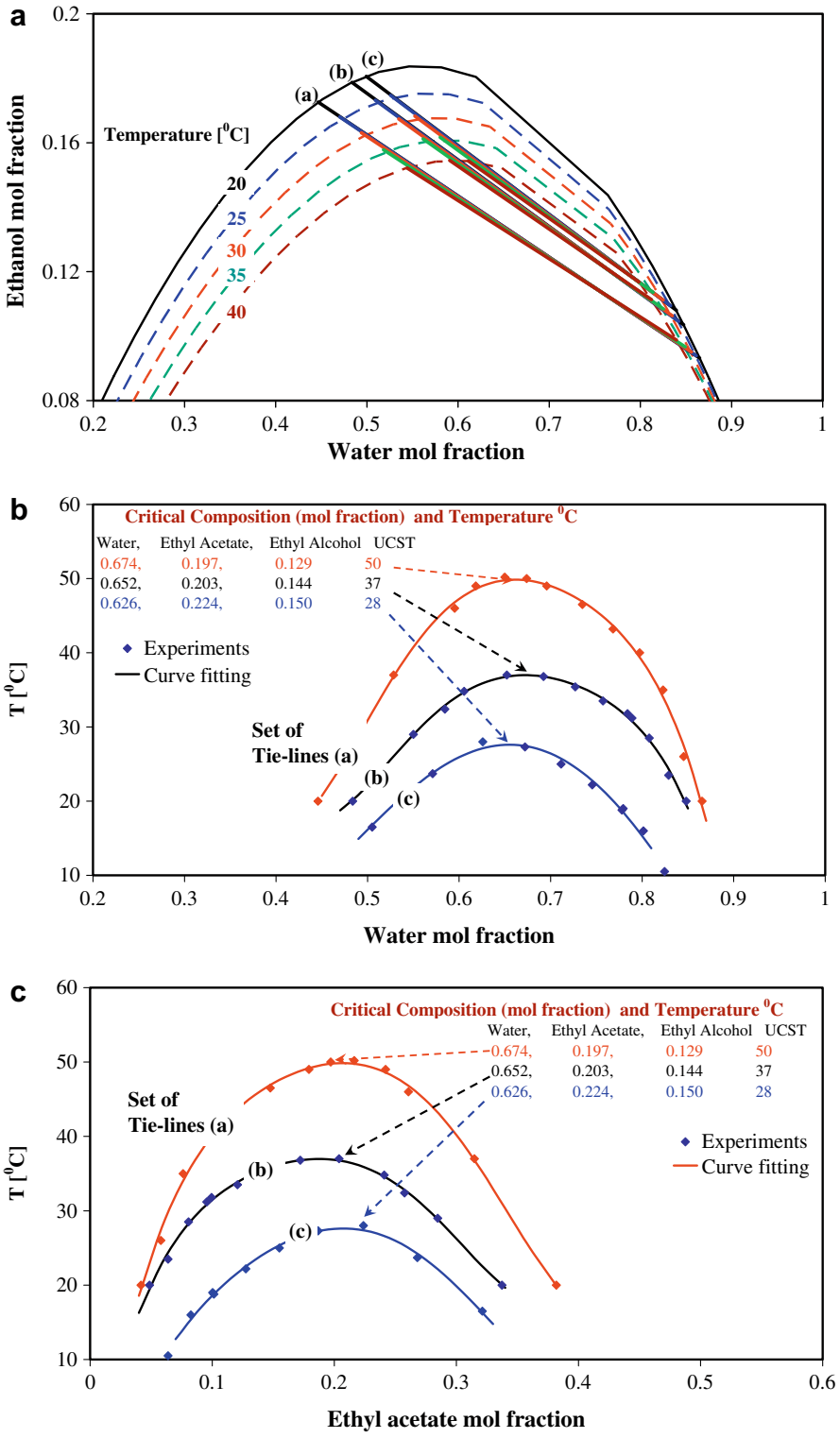

Fig. 2. Experimental coexistence (binodal) curves of the three solvents mixtures (related to three different sets of tie lines, *a*, *b*, *c*) used in the experiments: (a) effect of temperature variation on the tie-lines. Variation of composition with temperature corresponding to the three different sets of tie-lines (b) water composition, (c) ethyl acetate composition.

system are not available, and cannot be derived based on the available NRTL model parameters for this solvent mixture (see Appendix A). Based on the regular solution model [8] fitted to the UCST of the WEA solvent system (assuming a pseudo 2-C system), an estimate of the heat of mixing was obtained. This estimate yields $\Delta H_{\text{mixing}} > 0 \approx (5 \div 10\%)\ \Delta H_{\text{sensible}}$. In the absence of reliable values of ΔH_{mixing}, the heat transfer rates were determined based on the sensible heat only, which therefore results in conservative values for the experimental heat transfer coefficient. The errors in the experimental heat transfer coefficients resulting from the temperature and flow rate measurements, solvent composition and physical properties calculations were estimated to be in the range of 10–30% (the higher values are associated with experiments with small temperature difference).

Table 1a
Mixture compositions used in the experiments[a]

Tie-line		Water-rich	Critical comp.	Organic-rich	Water-rich	Critical comp.	Organic-rich
		Mole percentage (%mol)			Volume percentage (%vol)		
a	Water	74.7 (74.7)	64.2		39.3 (40.0)	28.0	
	Ethyl Acetate	13.6 (13.8)	22.4		39.3 (40.0)	53.0	
	Ethanol	12.4 (11.5)	13.4		21.4 (20.0)	19.0	
	T_{cp} (°C)	42 (46)	50		42 (46)	50	
b	Water	77.1	69.5	28.0	44.0	34.0	21.0
	Ethyl acetate	11.0	16.6	55.0	34.0	44.0	58.0
	Ethanol	11.9	13.9	17.0	22.0	22.0	21.0
	T_{cp} (°C)	32	37	32 (29)	32	37	32 (29)
c	Water	81.0			50.0		
	Ethyl acetate	9.0			30.0		
	Ethanol	10.0			20.0		
	T_{cp} (°C)	19 (18)			19 (18)		

[a] The data are related to the following experiments: cloud points, forced and free convective heat transfer, flow pattern visualization and macro-scale visualization. The values in the brackets refer to cloud point experiments in which the compositions were slightly different.

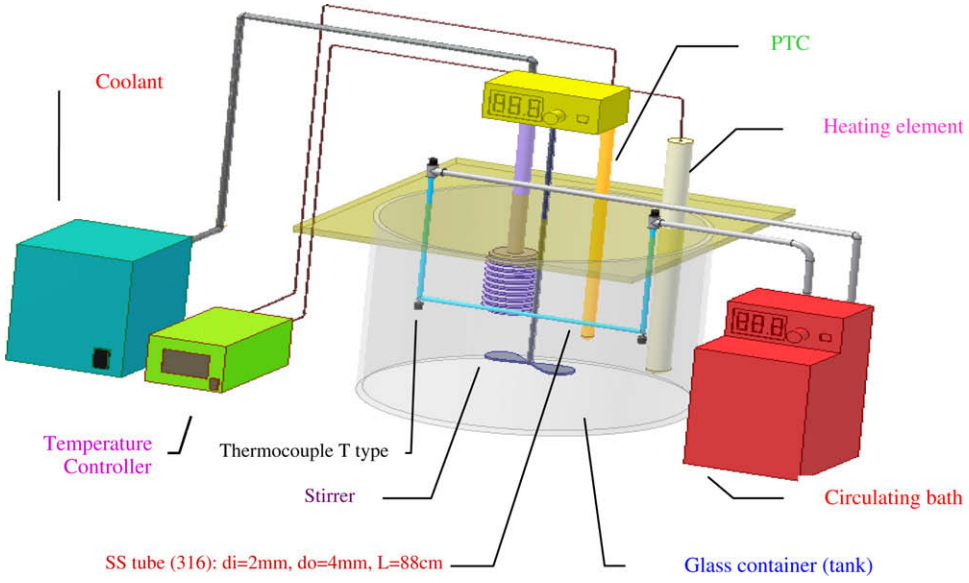

Fig. 3. Schematic description of the experimental setup.

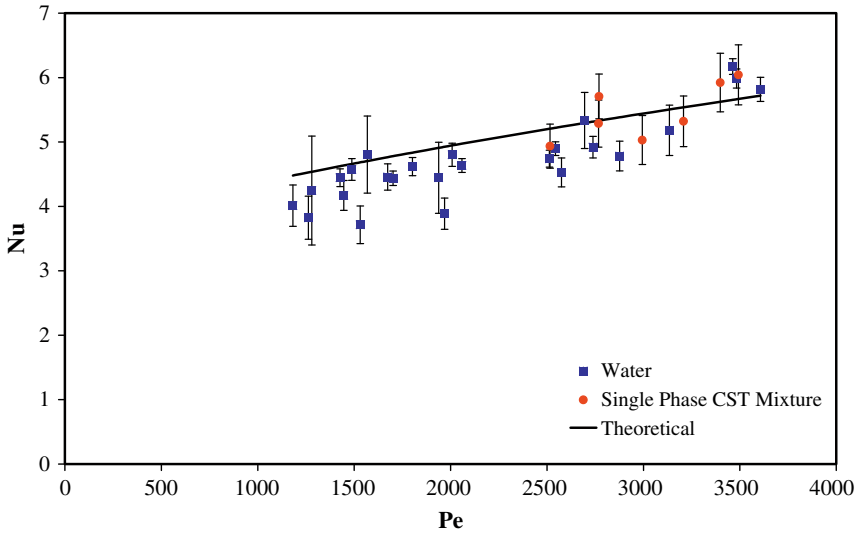

Fig. 4. Comparison between the experimental results for forced convection of water and single phase CST mixture with the predictions of Eq. (2).

The experimental setup and calculation procedure for obtaining the convective heat transfer coefficient were tested by conducting control experiments using single phase water flow and single phase flow of the CST mixture (above the cloud point). As shown in Fig. 4 the results were found to be reasonably predicted by using a well-established correlation [21] for the convective heat transfer in the thermal developing region (the flow in the test section is assumed to be fully developed laminar pipe flow):

$$Nu_D = 3.66 + \frac{0.0688(D/L)Pe}{1 + 0.04[(D/L)Pe]^{2/3}} \tag{2}$$

where D is the tube inner diameter and L is the length of the test section – the horizontal sections of the U-tube.

2.3. Experimental setup for free convection heat transfer

The same basic setup was used to conduct experiments on 'free convection' heat transfer from a cylindrical surface, namely the outer surface of the horizontal section of the U-shaped stainless steel (316) tube (outer diameter of 4 mm). When 'free convection' is being tested, the tank contains the solvent system, while water is circulated through the tube. The transparent tank enables visualizing the flow phenomena associated with the 'free convection'.

Although both the free convection and convective heat transfer experiments were conducted in the same apparatus, a different experimental procedure was used in the two cases. In the free convection experiments, the CST mixture in the tank was heated to a uniform temperature above the cloud point, T_{cp} using the temperature controller and the stirrer. To minimize evaporation losses the solvent mixture composition with the lowest UCST (≈28 °C) was used (set of tie-lines c in Fig. 2). The bulk temperature of the CST mixture in the bath was in the range of 23–26 °C.

The surface of tube was cooled by circulating cooling water through the tube, resulting in an average wall temperature in the range of 14.5–24.2 °C. Phase separation on the tube outside surface occurred when the wall temperature was below the cloud point. The overall composition of the CST mixture in the experiments was off-critical water-rich with 0.81 water, 0.09 ethyl acetate and 0.10 ethanol, molar fractions. It corresponds to cloud point temperature of about 17 °C. However, as a result of solvent evaporation during the experimental runs and recurrent composition adjustments, the actual cloud point varied between 17 and 21 °C. Obviously, the stirrer was switched off before starting the cold water circulation in the tube. However, since the heat capacity of the solvent mixture in the tank is relatively very high, its bulk temperature was practically maintained constant throughout the experimental runs.

The heat transfer rates were tested for various temperature differences between the tube surface and the bulk of the solvent mixture. As a reference, experiments were also conducted for similar temperature differences, however, when both the bulk and the pipe surface temperatures were above the cloud point temperature; namely, without phase separation. The experimental free convection heat transfer coefficients were calculated using the following equations:

$$Q = [\rho \cdot C_p \cdot \dot{V} \cdot (T_{out} - T_{in})]_{water}; \quad h = \frac{Q}{A_{out} \cdot (T_b - T_w)} \tag{3}$$

where $\dot{V}$ is the volumetric flow rate, A_{out} is the tube outer surface area, T_{in}, T_{out} are the inlet and outlet temperatures of the flowing water, T_w is the surface (average) temperature and T_b is the far field temperature in the tank. The water physical properties (ρ and C_p) were calculated at the average temperature.

The experimental setup and calculation procedure were tested by conducting control experiments for free convection heat transfer from a horizontal section of the U-tube while the tank is filled with pure water instead of the CST mixture. The results were found to compare well with the following well-established correlation for free-convection heat transfer form a constant surface temperature of a horizontal cylinder [22]:

$$Nu_D = \left\{0.6 + \frac{0.87Ra_D^{1/6}}{[1 + (0.599/\mathrm{Pr})^{9/16}]^{8/27}}\right\}^2;$$

$$Ra_D = \frac{g\Delta\rho D_o^3}{\mu\alpha}; \quad 10^{-5} < Ra_D < 10^{12} \tag{4}$$

A complementary experiment was conducted to study the 'free convection' from spherical geometry. A stainless steel ball with a thermocouple placed in its center was cooled in an incubator to a temperature below the cloud point, T_{cp}. The isothermal ball was then dipped in the stagnant hotter solvent system (above T_{cp}) and the flow around the ball was visualized.

2.4. Flow visualization

The transparent tank enables visualizing of flow phenomena associated with the natural convection from a cooled surface (cylindrical tube or sphere) immersed in a solvent mixture at a temperature above its T_{cp}. The flow phenomena associated with the free convection was recorded by a SONY CCD camera model DCR-TRV50E. To enable a better visualization of the flow of the two phases, which only slightly differ in their refraction index, a stripped background (white/pink) 3 mm wide was placed in the background.

2.5. Two-phase flow patterns

The characteristic flow pattern during isothermal flow of the analyzed solvent system in the pipe was also investigated in order to broaden the understanding of the experimental results. A simple experimental setup was designed in order to enable visualization of the flow pattern. A solvent system of a known composition and cloud point temperature was separated into two phases. The separated two phases are kept in 10-L containers equipped with valves. The flow rates were controlled by two rotameters (GILMONT Instruments) equipped with micro-capillary valves. Each of the rotameters was calibrated separately for the particular liquid phase.

The flow of the two-phases from the container is gravity driven, and they are introduced through a Y junction to the glass tube. The test section consists of a horizontal tube, of 70 cm length, ID = 2.3 mm and OD = 3.7 mm. The data were recorded by the CCD camera (SONY, model DR-TRV50E), augmented by external 10-fold magnifying lens. The pictures were taken 50 cm downstream the tube entrance to ensure developed flow. Similar flow visualization experiments were conducted in the horizontal section of a U-shaped glass tube, with the same geometry of the tube used in the convective heat transfer experiments. Under the same operational conditions the observed flow patterns were practically the same in the long horizontal tube and the U-shaped tube.

The solvent system used in the isothermal flow pattern visualization experiments correspond to set of tie-lines (a) with an UCST of 50 °C (see Fig. 2). The experiments were carried out isothermally at room temperature of 22 °C. The density and viscosity of the heavy (water-rich) phase were 935 kg/m^3, and 1.74 mPa s, and of the light (organic-rich) phase 890 kg/m^3, and 0.90 mPa s, respectively. Although the surface tension is low (≈0.004 N/m), due to the small tube diameter the system Eotvos number is estimated to be ($Eo_D = \Delta\rho g D^2/\sigma$) ≈ 0.7, hence the two-phase system is considered to be a capillary system [23]. The range of flow rates tested was 3–45 ml/min for each of the phases.

Visualization of the flow pattern during phase separation under non-isothermal (cooling) conditions was also attempted. To this aim, the glass U-tube was immersed in a square glass container (with flat walls to minimize optical distortion) filled with water at room temperature ($T = 20\ ^\circ C$). Here too, a stripped background was used to facilitate the distinction between the two phases. The solvent system of set of tie-lines (a) (see Fig. 2), with a volumetric composition of 40% water, 40% ethyl acetate and 20% ethanol, was used. This corresponds to a water-rich off-critical composition. The solvent system was heated above the T_{cp} (=42 °C) to form a single phase. Then, it was introduced into the cooled ($T = 20\ ^\circ C$) glass tube. The CCD camera (SONY DR-TRV50E) was used to visualize the flow.

2.6. Micro-scale visualization

To follow the separation process in the micro-scale, a Brightwell Technologies-Micro-Flow Imaging (MFI) model DPA4100 was used. The MFI platform integrates micro-fluidics, optical assemblies, digital image acquisition, and patented image analysis algorithms. The time interval between the images is controllable. The MFI is designed for characterization of particles in liquids and is used for particle analysis tasks (e.g., drug formulations, cell studies, drinking and waste water analysis). It is most effective for characterization of dilute slurries, and has never been used before to characterize the dynamics of particles growth in time. Therefore, the original working procedure [24] was adjusted for the present study purposes, and the system was operated under non-flowing conditions.

The test cell used is 400 μm in depth and 1760 × 1400 μm FOV (Field of View). The heated solution was inserted as a single phase to the test cell after it was thoroughly washed with the working solution and de-aerated. Then, its both ends were sealed tightly and the solvent was let to cool to the ambient temperature. Data were collected until the separation was completed, using a time interval of 1.2 s between two subsequent images. Droplet growth rate was estimated based on averaging the diameter of about 30 droplets of the 'same age'. The solvent mixture in the single phase stage was used as a reference in the image processing of the phase separation process.

As the MFI automatic image analysis is limited to dilute dispersion, it was used only as a mean for visualization and photo recording. The image analysis was conducted using Adobe Photoshop CS3 software. A standard sizing calibrated micro-sphere was used for sizing the drops.

The solvent mixtures used were those of tie-line set (b) (see Fig. 2). The separation processes associated with three compositions along this set of tie-lines were studied: critical composition, organic-rich and water-rich off critical compositions (see Table 1b).

3. Results and discussion

3.1. Convective heat transfer experiments

To obtain the convective heat transfer coefficient during phase transition, several experiments were conducted following the experimental procedure outlined in Section 2.1. The experimental results correspond to various flow rates of the solvent system in the pipe and different inlet temperatures and wall temperatures. The experimental heat transfer coefficient was calculated using Eq. (1.1).

The convective heat transfer was studied using two solvent systems with different UCST (sets of tie-lines a and b in Fig. 2). With these two systems the experiments were conducted with critical and off-critical (water-rich and organic rich) compositions (see Fig. 5). Table 1a summarizes the cloud points and the overall compositions of the mixtures used in the different experiments. The physical properties of the various solvent mixtures used in the experiments, at different temperatures, are calculated according to mixture compositions using available empirical relations (see Appendix B). Different phase separation mechanisms may be expected when the critical or off-critical compositions undergo temperature quench. In the former, the temperature quench is into the unstable region, resulting in spinodal decomposition. When cooling a mixture of off-critical composition below the cloud point, two successive mechanisms may occur: nucleation growth in the meta-stable region, which is then followed by spinodal decomposition (see Section 1). The quenching induced in the experiments was up to about 15 °C below the cloud point, T_{cp}.

The experimental results for the heat transfer coefficients were compared with the single phase Nusselt number (Nu_{sp}). The latter were calculated using Eq. (2) and correspond to the values which would be have been obtained without phase separation using the same solvent mixtures and at the same working temperatures. The augmentation of the heat transfer coefficient due to phase separation is defined by:

$$AF = \frac{Nu}{Nu_{sp}} = \frac{h}{h_{sp}} \tag{5}$$

Such presentation of the results enables to clearly display the heat transfer enhancement due to the phase separation process.

Obviously, the overall phenomena resulting from phase separation, including the secondary flows, the simultaneous primary flow, and the associated heat and mass transfer processes are rather complicated. However, it is known that in addition to the separation mechanism (spinodal vs. nucleation), the 'quenching depth' and the 'quenching rate' affect the rate of droplet growth and their velocities [18], and therefore, also the heat transfer rates. In the experiments conducted, the quenching depth is represented by $(T_{cp} - T_{out})$ and the quenching rate by $(T_{in} - T_{out})U/L$, where L/U is the residence time in the test section. The corresponding dimensionless time (normalized by D^2/α) is represented by $(Pe \cdot D/L)^{-1}$. The temperature differences are normalized by the maximal potential quench $(T_{cp} - T_w)$ associated with the phase separation for the specific mixture composition and wall temperature. Using these dimensionless variables, the experimental results for AF were found to be represented by the following empirical (dimensionless) correlation:

$$AF = 0.111\left(\frac{T_{in} - T_{out}}{T_{cp} - T_w}\frac{D}{L}Pe\right)^{0.75}\exp\left[1.9\left(\frac{T_{cp} - T_{out}}{T_{cp} - T_w}\right)^{3.6}\right] \tag{6}$$

All the experimental data used for deriving the parameter values of Eq. (6) correspond to conditions for which the phase separation took place throughout the entire text section, namely $T_{in} < T_{cp}$. Part of the data was left for the correlation validation. It is worth noting that the D/L in Eq. (6) evolves from the normalization of the residence time. However, as all the experiments correspond to the same D/L, its effect on AF could not be extracted from the data.

The comparison between the value predicted by Eq. (6) and the experimental AF is shown in Fig. 6a. The applicability of this correlation was tested via using $AF * h_{sp}$ to predict the outlet mixture

Table 1b
Mixture composition used for the micro-visualization experiments

	Water rich	Critical comp.	Organic rich
Water (%mol)	80.7	69.2	55.0
Ethanol (%mol)	11.2	13.6	16.5
Ethyl acetate (%mol)	8.1	17.2	28.5
Separation temperature (°C)	28.5	36.8	29

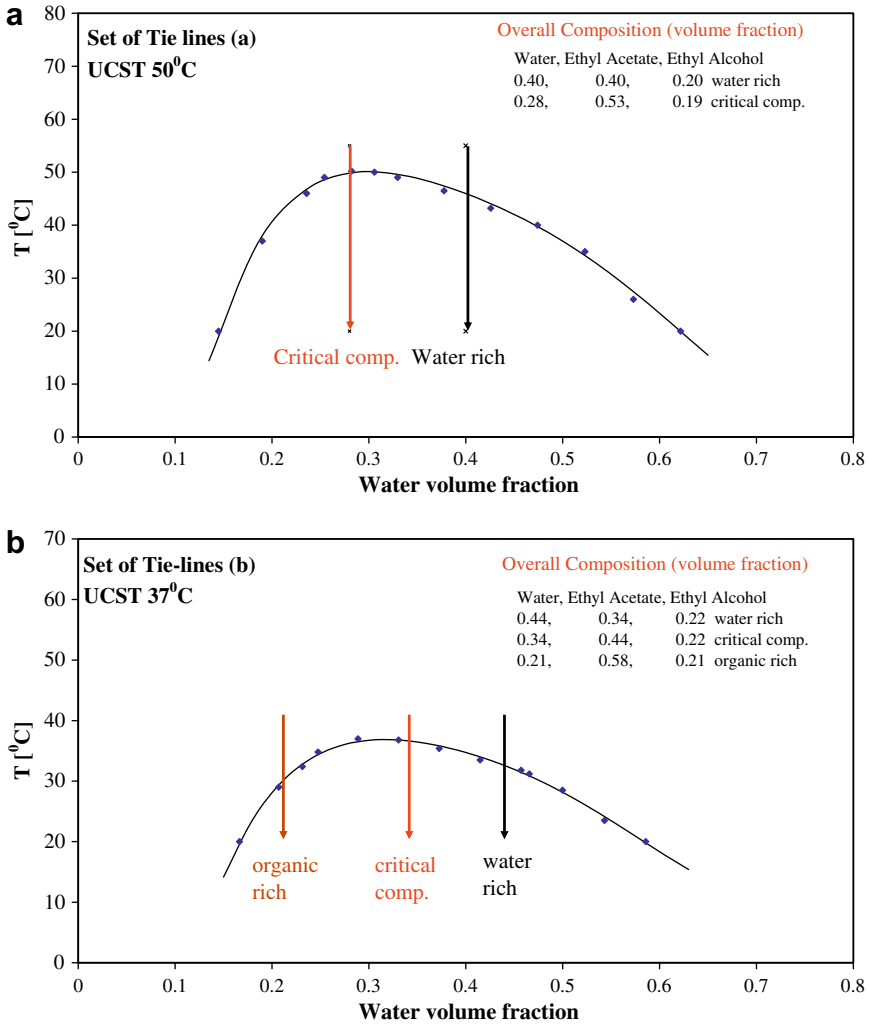

Fig. 5. Various overall compositions (volume fractions) of the mixtures tested in the convective heat transfer experiments: (a) set of tie-lines (*a*), (b) set of tie-lines (*b*) (see Fig. 2).

temperature (Fig. 6b). The latter validation is important, since the heat transfer coefficient is now dependent also on the quench rate, and therefore on the outlet temperature. Consequently, the calculation of T_{out} requires solving an explicit algebraic equation (see Eq. (1.1)).

Generally, as shown in Fig. 6a, the phase separation affects the convective heat transfer coefficient compared to the corresponding single phase values. The largest *AF* values are obtained for organic-rich compositions, where phase separation augments the heat transfer coefficient by 50% to 130%. With the water-rich off-critical compositions the *AF* values are lower (in some case lower than 1). On the other hand, with a critical composition, in most of the cases the phase separation was found to attenuate the convective heat transfer coefficient ($AF < 1$). As may be noticed, the agreement of data of the critical composition with correlation Eq. (6) is less favorable. This may be expected, as the phenomenon involved in phase separation of mixtures with critical compositions is quite different from that associated with separation of off-critical mixtures (spinodal decomposition vs. nucleation growth). Indeed, the empirical correlations for the *AF* could be improved if different parameter values are fitted to the critical composition (results are not reported here).

It can be postulated that augmented heat transfer rates during phase transition result from the lateral (in addition to the axial) velocity component induced by the motion of the separating and growing droplets during the phase separation process. Assuming the existence of such a lateral velocity component (), the ratio between the associated convective heat transfer to that obtained under single phase flow conditions (represented by Eq. (2), with $St = Nu/Pe$) can be approximated by $AF \approx v/(USt)$. Using the experimental *U*, *St* and *AF* yields values of of about 1 to 5 mm/s for the cases of $AF > 1$.

As discussed above, with off-critical composition, the phase separation during temperature quench is a dynamic process, associated with droplet growth and movement. The movement of the small droplet (smaller than the capillary length, $\sqrt{\sigma/g\Delta\rho}$, of the order of 1 mm) is not gravity dominated, but driven by the chemical potential gradient [25]. The measured velocity of the micro-droplets in the unstable region was reported to be in the range of = 0.1–1 mm/s [18,19,26], with droplet growth proportional to *t*. These droplet velocities are of the same order of magnitude as the lateral velocities required for obtaining $AF > 1$.

Most of the droplets growth and droplet velocities reported in the literature refer to two-component systems, or pseudo two-component systems (i.e., minute concentration of the third component); nevertheless, similar results were observed during the separation of the three-component solvent system used in the present study. Fig. 7 shows typical pictures obtained for

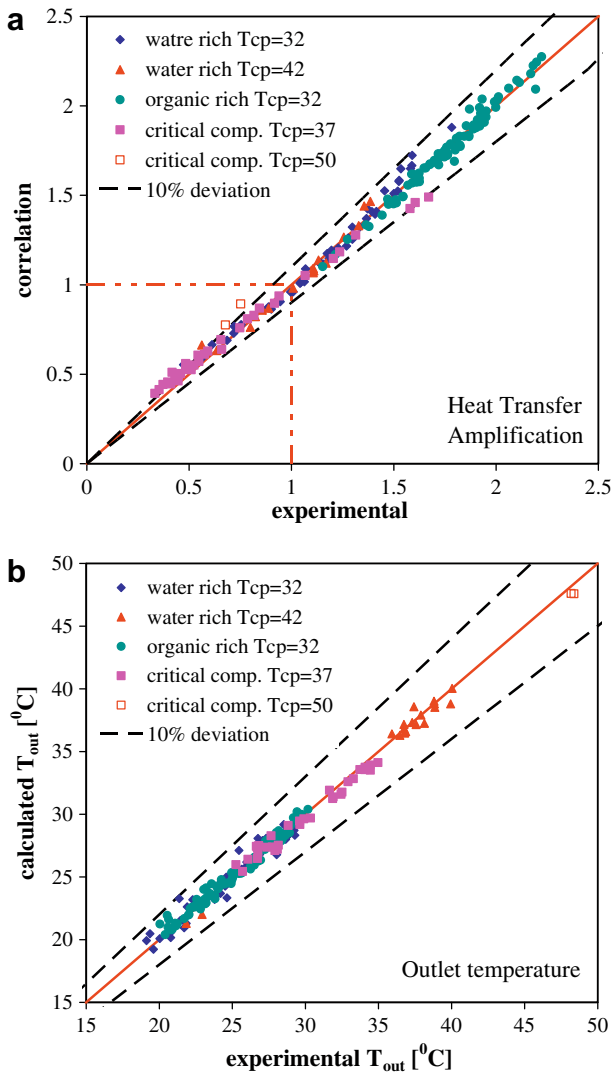

Fig. 6. (a) Comparison of the correlation (Eq. (6)) with the experimental results for the heat transfer amplification for convective heat transfer with phase transition for different compositions and wall temperatures. (b) Comparison of the calculated outlet mixture temperature (using $AF * h_{sp}$) with the experimental results for different compositions and wall temperatures.

off-critical and critical quench into the unstable region taken by the Micro-Flow Imaging (MFI) apparatus. The pictures shown are part of sequential set of pictures, which enable an estimation of the droplet velocity and its growth rate. In the case of critical composition, we could not measure the 'domains' size during the initial stage of the phase separation, and the data shown in Fig. 8 correspond to the late stage of phase separation, where the boundaries of the domains could be clearly identified ($t > 250$ s). For off-critical quench, two different stages of droplets growth were definitely observed. In agreement to the rates reported in the literature (see Section 1), the initial growth rate (diffusion stage) was found to be characterized by d proportional to $t^{1/3}$, and d proportional to t^1 in the second (convective) stage (see Fig. 8). The corresponding growth rate in the second stage (derivative of the radii with time) is about 0.1 μm/s for both the off-critical and critical compositions. This value is in a general agreement with the findings reported by Poesio et al. [18] for low quenching rates. The latter demonstrated a strong dependence of the droplet growth rate on the quenching rate. Unfortunately, the MFI measurement system does not allow a control of the quenching rate, which was rather low (gradual cooling to the ambient temperature). However, with the quenching rates typical to the convective heat transfer experiments of the present study (1–7 °C/s for off-critical compositions) the drop growth rate is expected to be much (two orders of magnitude) higher. It is worth noting that part of the large drops (of about $d = 100$ μm) were observed to adhere to the walls of the measurement test cell and remained motionless. The growth rate of those drops was found to be proportional to $t^{0.5}$.

Visual inspection of the sequential pictures enables an estimation of a typical value for the droplet movement velocity in the bulk of the separating mixtures during quenching of off-critical mixture composition (see for example Fig. 7b). The movement velocity was found to be of the order of 0.1 mm/s, which is in the lower range of the velocities reported in the literature, as mentioned above. Similarly to the slow growth rate, this may also be a result of the low quenching rate in the MFI apparatus. However, it is worth noting that the drop velocity could be measured only for frames containing a small amount and of relatively large droplets, and may not be representative of the droplet velocity throughout the entire separation process.

Similar visual inspection of the sequential pictures taken for (close to) critical composition (that is associated with the maximum temperature of tie-line set (b) (see Fig. 2) revealed a different structure of the growing domains of the separating phases (snap shots are shown in Fig. 7a); in this case, droplets similar to those observed during separation of off-critical compositions cannot be observed, although a pattern of interconnected domains (as reported in the literature [18,19]) cannot be clearly visualized in the pictures either. A growth stage of d proportional to t^1 (similar to that observed with the off-critical compositions for the convective stage) was identified, but the initial growth stage could not be characterized with the MFI apparatus. It is important to note that the domains appeared to be rather motionless during most of the separation period. This finding can explain the fact that heat transfer rates were the lowest for the mixture of a critical composition, and that phase separation in some cases may have an adverse effect ($AF < 1$) on the heat transfer rates compared to single-phase flow.

The highest heat transfer amplification was obtained for the case of organic-rich off-critical composition (see Fig. 6a). Unfortunately, at this stage no definite explanation for this finding was found. The differences between the AF values corresponding to water-rich and organic-rich are relatively small. They may be related to different heat of mixing associated with the water-rich and organic-rich compositions of the solvent system studied (which was not accounted for in the heat transfer calculations). Different lateral droplets velocities during the separation of off-critical organic-rich and water-rich compositions may also affect the AF. However, since we were able to measure the droplet velocities only during the late stages of the phase separation, we could not substantiate this hypothesis via a comparison of the droplets velocities of off-critical organic-rich and water-rich compositions. Another reason could be the identity of the phase covering the wall following phase separation. However, picture taken in the pipe during phase separation (e.g. Fig. 9b) could not shed light on this issue.

Although the empirical correlation (Eq. (6)) implies that the AF is reduced at long residence time (low PeD/L), the heat transfer phenomena associated with a very long residence time (i.e., long test section) was not tested in the present study. While it is expected that the effect of phase separation diminishes in long tubes, the heat transfer coefficient will not be the same as that obtained in single phase flow (i.e., $AF = 1$). With the resulting liquid–liquid two-phase flow, the heat transfer coefficient is dependent on the two-phase flow pattern, which in turn, is dependent on phases flow rates and properties.

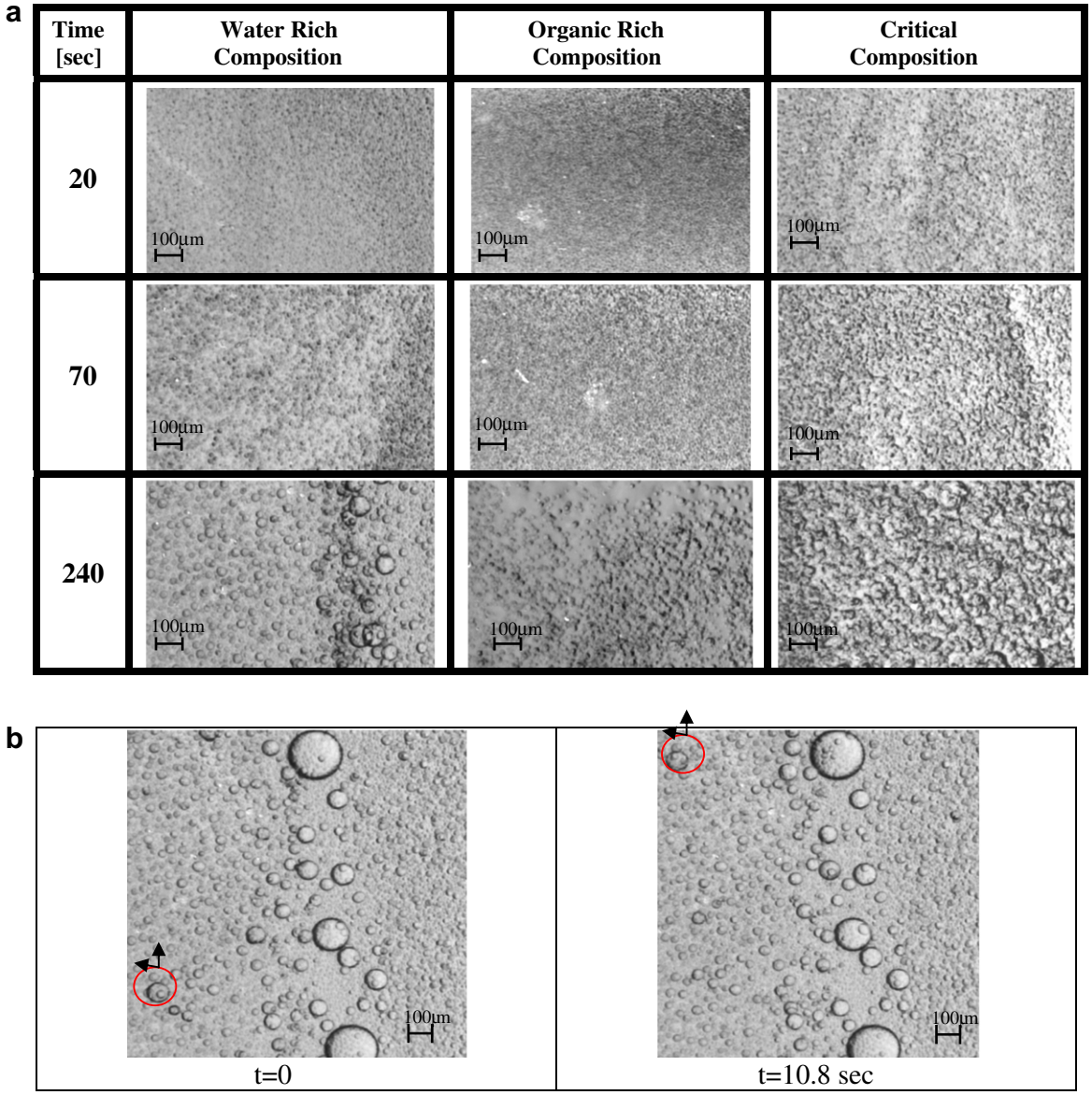

Fig. 7. (a) Micro-visualization of the droplets growth following a temperature quench of critical and off-critical CST mixtures based on set of tie-lines (b). (b) Demonstration of the droplet movement during phase separation (water-rich mixture of tie-line set (b)). Note that only the velocities of the small drops were measured as the large drops adhere to the cell surface and are practically motionless.

3.2. Two-phase flow characteristics

The characteristic flow patterns (under isothermal conditions) observed in horizontal tube for various phases flow rates are shown in Fig. 9a. The flow patterns observations were made at the same total flow rate range of the heat transfer experiments, and for various heavy-to-light phase flow rate ratios. In most of the cases, the observed flow pattern corresponds to bubbly flow, or elongated-bubble flow, with bubbles length ranging from a size smaller than the tube diameter, to very long bubbles, of the order of the test section length. The observed flow patterns can be categorized into four main flow patterns: plug flow (elongated light phase bubbles), bubbly flow (light phase bubbles), inverted plug flow (elongated heavy phase bubbles) and inverted bubbly flow.

Nevertheless, the flow pattern in the test section of the convective heat transfer experiments is not expected to be the same as that obtained under isothermal conditions even for the same total mixture flow rates. This is due to the continuous phase separation throughout the test section. Fig. 9b shows a typical picture of the flow pattern observed in the glass tube during phase separation. The small droplets formed during the phase separation actually occupy the entire tube and the flow pattern appears as a mist.

3.3. Free convection experiments

Some experiments were performed to test the potential of heat transfer enhancement in the case of free convection following the procedure described in Section 2.2. The experiments were limited to water-rich composition corresponding to tie-line set (*c*) (see Fig. 2 and Table 1a). A picture showing the flow phenomenon associated with the free convection from a cylindrical surface during phase separation (on the tube outer surface) is given in Fig. 10a. A distortion of the background (white/pink) stripes indicates the location of the two liquid phases of different refractive indexes.

It is worth recalling that in the experiments, an UCST solvent system was used, and therefore, in these experiments, the cylinder surface temperature is lower than the solvent bulk temperature. As long as the surface temperature is kept above the cloud point

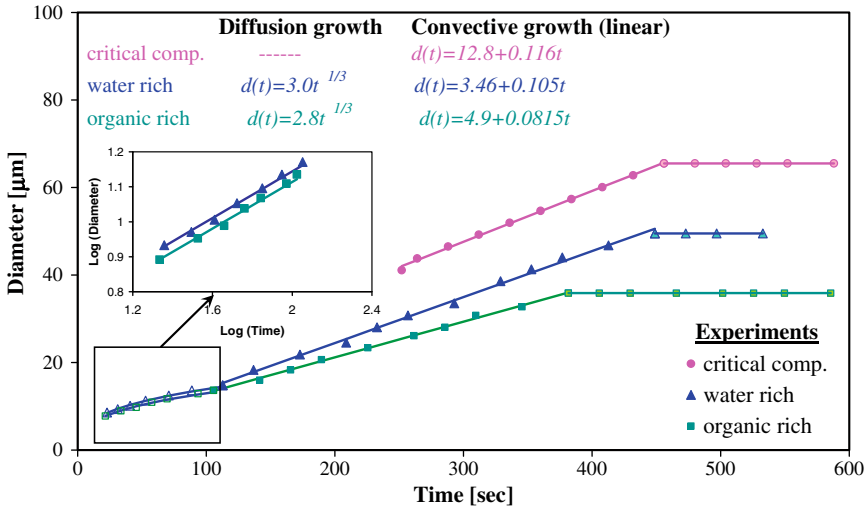

Fig. 8. Droplet growth rates for critical and off-critical compositions based on set of tie-lines (b). The droplet diameters are estimated based on averaging the diameter of about 30 droplets of the 'same age'.

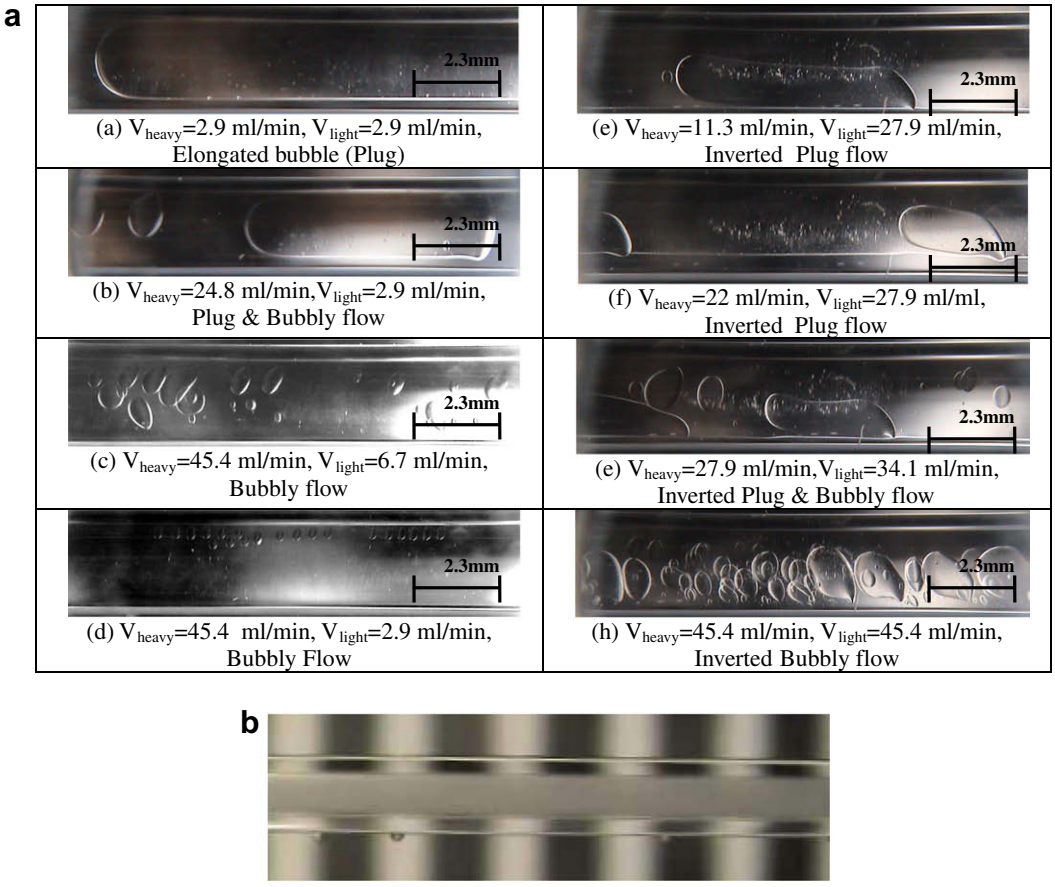

Fig. 9. (a) Liquid–Liquid flow patterns in isothermal (at 22 °C) flow of the two separated liquid phases of set of tie-lines (a) in the horizontal pipe. (b) Flow pattern during phase separation (non-isothermal flow, water-rich of tie-line set (a)).

temperature (T_{cp}), a conventional free convection due to temperature difference takes place. This temperature induced free convection could not be observed or pictured. However, when the temperature of the wall is equal or lower than T_{cp}, the inception of phase separation is visualized. A thin film of the heavy phase is formed over the tube surface, which drains down to form a thin 'curtain' that can easily be observed in the picture (Fig. 10a). This visualized flow phenomenon resembles that observed in vapor condensation over a cooled tube surface. However, in the phase separation experiments, the formation of the heavy phase 'curtain' is accompanied by separation of the light phase, which moves upward. The separated light phase does not form a continuous 'curtain', and is more difficult to be visualized. Indeed, as off-critical composition with water-rich composition was used, the volume

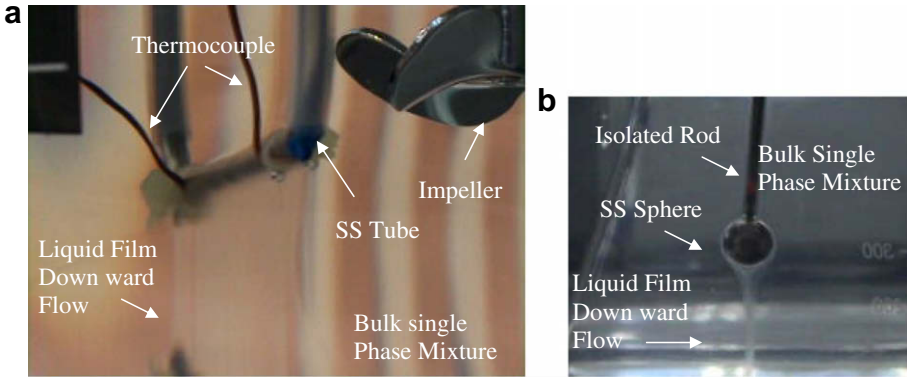

Fig. 10. Free convection visualization: (a) from horizontal tube, (water-rich composition of tie-line set (c), T_{cp} = 19 °C, T_b = 23–26 °C, T_w = 16–24 °C). (b) From sphere (water-rich of tie-line set (a), T_{cp} = 42.5 °C, T_b = 46 °C, T_w = 35 °C).

of the heavier, water-rich phase, during separation is much larger than that of the lighter, organic-rich phase (see Fig. 12(a)).

A similar flow phenomenon was obtained when a cooled sphere was introduced into the hotter solvent mixture (see Fig. 10b). In this geometry, the upward flow of the separating lighter phase can be more easily detected. Visualization experiments were repeated with another solvent composition of a higher CST of 42 °C, and basically the same flow phenomena were observed.

The experimental Nusselt number obtained in free convection from the cylindrical surface vs. the difference between the bulk temperature and the average wall temperature is depicted in Fig. 11. In this figure, a distinction is made between cases where the wall temperature was above the cloud point (no phase separation took place), cases where the wall temperature along the whole test section was definitely below the cloud point (phase separation took place over the entire surface), and cases where the average wall temperature was close to the cloud point (the temperature of only part of the surface was below the cloud point). For a reference, the corresponding calculated values for single phase free convection (Eq. (4)) are also shown for water (curve *A*). Two experimental points obtained for free convection in water surrounding for the maximal and minimal experimental temperature difference range are also shown, indicating the reliability and validity of the experimental setup and procedure.

Curve *B* in Fig. 11 shows the theoretical free convection *Nu* numbers obtained for the single-phase of the three component CST mixture (according to the temperature induced density difference of the mixture, see Fig. 12(b)). Obviously, curve *B* is valid only in case the temperature quench is outside the binodal curve, and phase separation does not occur (in the current experiments this correspond to $T_b - T_w < 6$ °C). As shown in the figure, the experimental *Nu* numbers corresponding to free convection in the single phase CST mixture are in a reasonable agreement with the predicted curve *B*. Obviously, some inherent scattering is associated also with the single phase experimental Nu_D values shown in Fig. 11, since different T_f values and compositions (i.e., different physical properties, Appendix B) in experiments are associated with the same $T_b - T_w$. The estimated error in the Nu_D values (via error propagation of temperature measurement and solvent composition) is generally about 10%. However, for the small temperature differences the estimated error is higher (up to 30%).

Fig. 11 clearly shows that in free convection the phase separation enhances the heat transfer rates by about 100%. The highest *Nu* values correspond to conditions where the phase separation occurred over the entire surface of the test section and for the highest temperature difference.

The potential for free convection heat transfer enhancement due to phase separation is shown by curve *C* in Fig. 11. The latter was calculated based on Eq. (4), where the density difference is taken as the difference between the heavy and the light phase densities at the average experimental wall temperature. As curve *C* is relevant only under conditions of phase separation

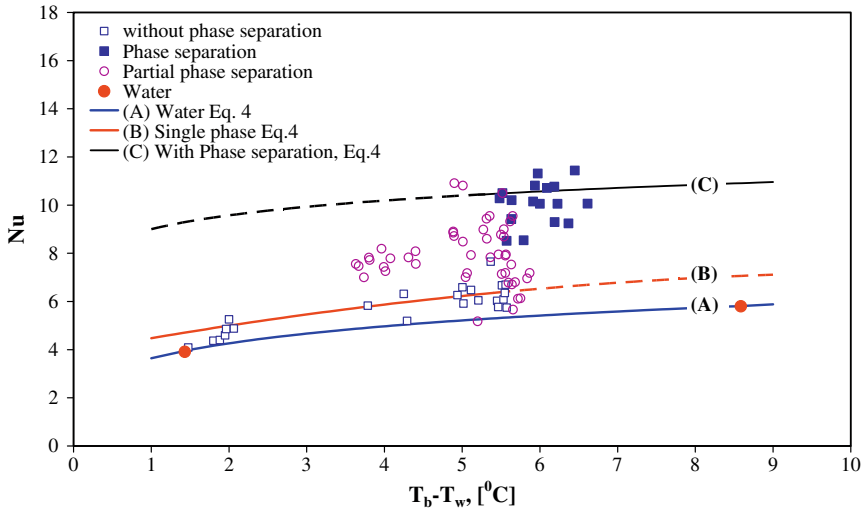

Fig. 11. Experimental results for natural convection with and without phase separation.

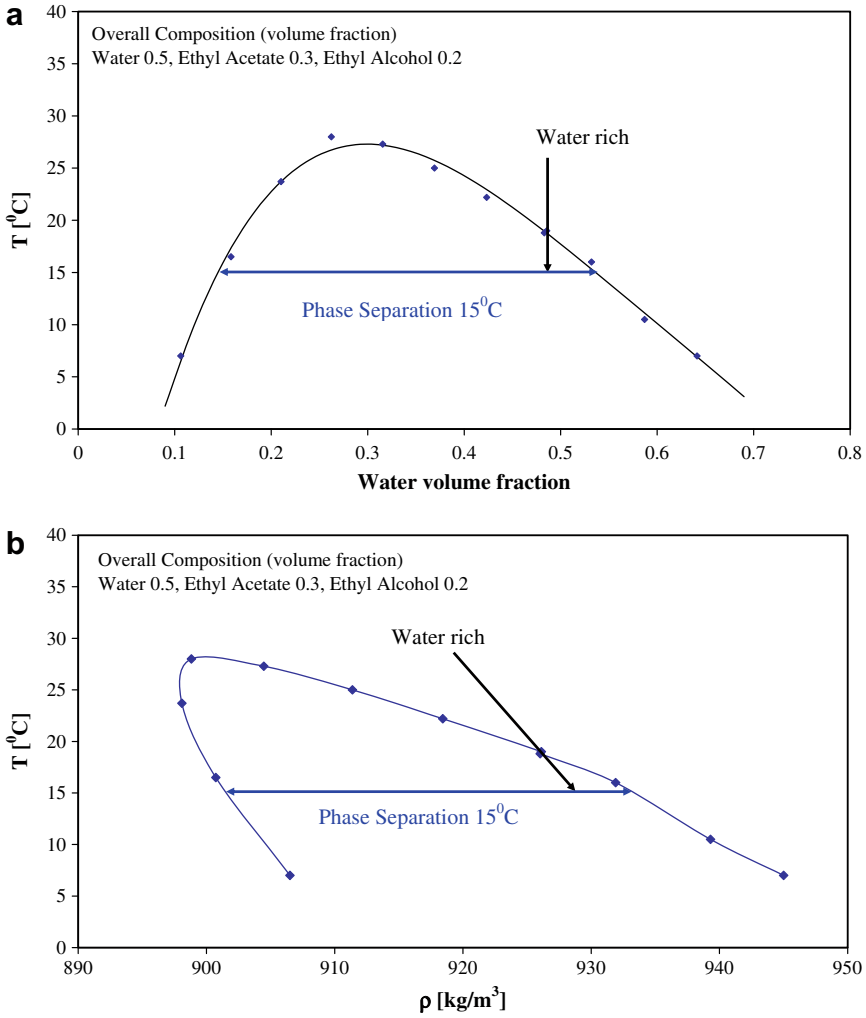

Fig. 12. Equilibrium water volume fraction (a) and density (b) variation with temperature of the coexisting phases of set of tie-lines (c). The water volume fraction and the density of the mixture used in the free convection experiments are also plotted.

($T_b - T_w > 5.5$ °C in the experiments), its extension outside of this range is represented by dashed line. Fig. 11 shows that the free convection *Nu* number in case of phase separation is reasonably predicted by considering the density difference between the separated phases as the process driving force. Obviously, the experimental results in the case of phase separation exhibit a larger scatter as compared to single phase conditions. This should be expected, since the free convection driving force is sensitive to variations in the CST mixture binodal curve (see Fig. 12) and the wall temperature that differ in the various experimental runs. Again, these variations of the driving force are not represented by the abscissa of Fig. 11. This inherent scattering is also characterizing the calculated values (Eq. (4)), and consequently curve *C* actually represents a curve fit to some scattered calculated values. Note that the liquid properties (used in Eq. (4)) were calculated based on the overall CST mixture composition at the film temperature (although the liquids around the tube surface are separated phases).

The results of this experimental study show that on the macroscale, the free convection heat transfer phenomena (in contrast to the convective heat transfer) are dominated by gravity, even in the case of phase separation. The observed enhancement of the heat transfer rates is related to the increased effective density difference during phase separation.

4. Conclusions

In this study convective heat transfer and flow phenomena during liquid–liquid phase separation were investigated experimentally. These phenomena involving heterogeneous phase separation and the associated heat transfer mechanism have not been yet investigated in the literature. The heat transfer rates obtained with phase separation were compared with those obtained under the same flow conditions of single-phase liquid of the solvent system. The results support the premise that heat transfer coefficient can be augmented by inducing liquid–liquid phase separation.

The heat transfer rates were studied for convective heat transfer in a small diameter horizontal tube and free convection from its outer surface. It was found that with phase separation the forced convection heat transfer coefficients can be improved by up to 130%. Higher augmentation of the forced convection heat transfer rates were obtained with off-critical compositions; whereas with mixtures of critical compositions the heat transfer coefficient may even be deteriorated during phase separation. The free convection phenomena from the outer surface were studied only with an off-critical mixture. In this case the heat transfer coefficients were found to be augmented by up to 100% compared to free convection in single phase liquid.

Macro- and micro-flow visualization were also conducted to follow the flow phenomena during the phase separation. These experiments show that the phase separation of the 3-component system resembles the universal droplet growth rate, namely, proportional to $t^{1/3}$ in the initial growth (diffusion) stage, and proportional to t^1 in the second (convective) stage. The characteristic surface tension driven droplet velocity was also observed.

In forced convection heat transfer in horizontal pipe flow, the heat transfer augmentation is attributed mainly to the lateral movement of the separating droplets, which affects mixing of the fluid near the heat transfer surface. This lateral velocity is not necessarily gravity dominated, in particular for small droplets, as it is driven by the chemical potential gradients existing under non-equilibrium conditions. Indeed, an estimate of the lateral velocity scale required to yield the measured heat transfer augmentation, resulted in velocities that are of the same order of magnitude as those measured in non-flowing conditions (closed cells [20]). On the other hand, the augmentation of the free convection from the outer surface is found to be mainly gravity driven. The augmentation is a result of the larger density difference of the separating phases, as compared to single phase free convention for the same temperature difference.

Appendix A

A three component system is represented by a three dimensional surface, reflecting the variation of temperature and the compositions of two of the components. The equilibrium compositions of the two separated phases at a given temperature are represented by tie-lines. Any mixture with an overall composition along a tie-line will separate into two coexisting phases, and their equilibrium compositions are represented by the two external points of the tie line. The length of the tie lines varies with the overall composition and vanishes at the plait point. The equilibrium compositions of the coexisting phases are temperature dependent and can be represented by a different set of tie lines for each temperature. The tie-lines of UCST systems become shorter as the temperature is elevated (see Fig. 2(a)).

In general, the NRTL equation (Eq. (7)), or a similar model, can be used to obtain the coexisting concentrations of the two liquid phases:

$$\begin{aligned}
&\ln\gamma_i = \frac{\sum_{j=1}^{m}\tau_{ji}G_{ji}x_j}{\sum_{l=1}^{m}G_{li}x_l} + \sum_{j=1}^{m}\frac{x_jG_{ij}}{\sum_{l=1}^{m}G_{lj}x_l}\left(\tau_{ij} - \frac{\sum_{n=1}^{m}x_n\tau_{nj}G_{nj}}{\sum_{l=1}^{m}G_{lj}x_l}\right);\\
&\tau_{ji} = \frac{(g_{ji}-g_{ii})}{RT};\ G_{ji} = \exp(-\alpha_{ji}\tau_{ji})\\
&\tau_{ii} = \tau_{jj} = 0;\ G_{ii} = G_{jj} = 1
\end{aligned} \tag{7}$$

Experimental data for the water–ethanol–ethyl acetate system, as well as the NRTL and UNIQUAC model parameters are reported in the literature [27–29]. However, the data do not cover the combinations of temperatures and compositions used in the present experiments. Moreover, using the reported NRTL (and UNIQUAC) model parameters fails to predict the existence of phase transition (in most cases), in few cases the cloud point temperature is largely over predicted. Therefore, we conducted a series of experiments to obtain data on the composition of the coexisting phases and the phase transition temperatures for solvent compositions used in our experiments. It is worth noting that direct measurement of the composition of solvent system that contains water is difficult to conduct with a Gas-Chromatograph, which is the conventional analytical tool used for concentration measurement of organic solvents.

Analysis of equilibrium compositions predicted by the NRTL model for a specified overall composition revealed that all tie lines associated with this composition (at different temperatures) are practically parallel (namely all these tie-lines share a common plane, see Fig. 2(a)). This observation enables to adopt a simplified and convenient procedure to obtain the equilibrium compositions at different temperatures for various overall compositions of the solvent system that are associated with a specified set of tie-lines (which share a common plane).

The procedure is based on the well-known and reliable cloud point experiment. The latter is conducted in the following way:

a. Preparing a mixture with a known composition.
b. Heating, while mixing, and recording the temperature at which the solution becomes clear (T_{cp}).
c. Validation of the T_{cp}, by cooling the mixture and recording the temperature for which the solution becomes opaque.

Based on the finding that the tie-lines are parallel at different temperatures, it is sufficient to have data on the equilibrium compositions of one tie-line at a single temperature. Accordingly, the following procedure was used to obtain the equilibrium compositions corresponding to the set of tie-lines (at different temperatures):

a. A mixture of known overall composition is prepared and well mixed at a temperature of 20 °C (or 7 °C for set of tie-lines (*c*)), and then the two coexisting phases are separated (in a separating funnel).
b. Their composition was determined using the NRTL model for which reliable data and parameter values are available at 20 °C. The NRTL model parameters at different temperatures can be found in the literature [27–29].
c. Different mass ratios of the two-phases were taken to obtain different compositions along the tie-line.
d. For each of those compositions, a cloud point experiment (see above) was conducted to define its T_{cp}. The results of the variation of the water and ethyl acetate compositions with temperature are depicted in Fig. 2b and c for three different set of tie-lines used in our experiments. The maximal phase transition temperature of the solution is different for each set of tie-lines and is considered here as the "CST", similarly to the CST of binary systems.

The procedure was verified by using freshly prepared solutions of compositions obtained in step (c) (and differ from that of step a) and checking its T_{cp} independently. The so-obtained cloud point was found to be the same (within the error bounds affected by weight and temperature measurement errors) to that obtained in step (d).

In fact, the procedure used enables obtaining equilibrium data based on a limited reliable data of equilibrium compositions of the system at a single temperature.

Appendix B

The physical properties of the pure components at different temperatures were calculated based on empirical relations [30–39]. The empirical relations are summarized in Table B1. The properties of the mixtures were calculated based on the mass fraction of the components. The mixture viscosity was corrected according to [40]. The mixture density was not corrected for the mixing effect as the excess molar volumes of the components at the experimental compositions and temperatures are negligible [40].

Table B1
Empirical relations for the pure components physical properties at different temperatures [30–39]

Property	Empirical relations
Water	
ρ (kg m^{-3})	$1000\,(1-(T+288.9414)/(508929.2\times(T+68.12963))\cdot(T-3.9863)^2)$, T (°C)
C_p (J kg^{-1} °C^{-1})	$\frac{C_{p,w}(T\,^\circ C)}{C_{p,w}(15\,^\circ C)} = 0.996185 + 0.0002874\left(\frac{T+100}{100}\right)^{5.26} + 0.011160\times 10^{-0.036\,T}$ (°C)
	$C_{p,w}$ (15 °C) = 4185.5 k
k (W m^{-1} °C^{-1})	$k_w = -0.00000517T^2 + 0.0020083T + 0.559900$, T (°C)
μ (N s m^{-2})	$\mu_w = 0.0014793e^{-(0.0190798\cdot T)}$, T (°C)
Ethyl acetate	
ρ (kg m^{-3})	$\rho_{EtAc} = 1.99860 - 6.24971\times 10^{-3}T + 8.53568\times 10^{-6}T^2$, T (K)
C_p (J kg^{-1} °C^{-1})	$C_{p,EtAc} = 0.0143T^2 + 1.8552T + 1875.6$, T (°C)
k (W m^{-1} °C^{-1})	$k_{EtAc} = -0.000288T + 0.148622$, T (°C)
μ (N s m^{-2})	$\mu_{EtAc} = 0.0005323e^{-(0.0094982\cdot T)}$, T (°C)
Ethanol	
ρ (kg m^{-3})	$\rho_{EtOH} = -0.0013T^2 - 0.778T + 805$, T (°C)
C_p (J kg^{-1} °C^{-1})	$C_{p,EtOH} = 0.0891T^2 + 6.7708T + 2228.7$, T (°C)
k (W m^{-1} °C^{-1})	$k_{EtOH} = -0.000266T + 0.169548$, T (°C)
μ (N s m^{-2})	$\mu_{EtOH} = 0.0016276e^{-(0.0163210\cdot T)}$, T (°C)

References

[1] A. Bejan, Convection Heat Transfer, 2nd ed., Wiley, New York, 1995.
[2] J.G. Collier, J.R. Thome, Convective Boiling and Condensation, 3rd ed., Oxford University Press, Oxford, 1994.
[3] P.A. Kew, K. Cornwell, Correlations for prediction of boiling heat transfer in small-diameter channels, Appl. Therm. Eng. 17 (1997) 705–715.
[4] S.G. Kandlikar, Fundamental issues related to flow boiling in mini-channels and micro-channels, Exp. Therm. Fluid Sci. 26 (2–4) (2002) 389–407.
[5] J.R. Thome, State-of-the-art overview of boiling and two phase flow in micro channels, Heat Trans. Eng. 27 (2006) 4–19.
[6] A.W. Francis, Critical Solution Temperatures, American Chemical Society, Washington, 1943.
[7] C.H.P. Lupis, Chemical Thermodynamics of Materials, Elsevier, New York, 1983.
[8] S.M. Wallas, Phase Equilibria in Chemical Engineering, Butterworth publishers, London, 1985.
[9] R. Mauri, F. Califano, E. Calvi, Convection-driven phase segregation of deeply quenched liquid mixtures, J. Chem. Phys. 118 (19) (2003) 8841–8846.
[10] J.E. Farrell, O.T. Valls, Spinodal decomposition in a two dimensional fluid model, Phys. Rev. B 40 (10) (1989) 7027–7039.
[11] A. Ullmann, liquid–liquid extraction using solvent mixtures with a critical point of miscibility, Ph.D. Thesis, City College, New York, 1993.
[12] A. Ullmann, Z. Ludmer, R. Shinnar, Phase transition extraction using solvent mixtures with a critical point of miscibility, AIChE J. 41 (3) (1995) 488–500.
[13] R. Mauri, R. Shinnar, G. Triantafyllou, Spinodal decomposition in binary mixtures, Phys. Rev. E 53 (3) (1996) 2613–2623.
[14] N. Vladimirova, A. Malagoli, R. Mauri, Diffusion driven phase separation of deeply quenched mixtures, Phys. Rev. E 58 (6) (1998) 7691–7699.
[15] S.A. Vitale, J.L. Katz, Liquid droplet dispersions formed by homogeneous liquid–liquid nucleation: the ouzo effect, LANGMUIR 19 (10) (2003) 4105–4110.
[16] A.G. Lamorgese, R. Mauri, Nucleation and spinodal decomposition of liquid mixtures, Phys. Fluids 17 (2005) 034107/1–034107/10.
[17] N. Vladimirova, A. Malagoli, R. Mauri, Two dimensional model of phase segregation in liquid binary mixtures, Phys. Rev. E 60 (6) (1999) 6968–6977.
[18] P. Poesio, G. Cominardi, A.M. Lezzi, R. Mauri, G.P. Beretta, Effects of quenching rate and viscosity on spinodal decomposition, Phys. Rev. E 74 (2006) 011507/1–011507/13.
[19] J.C. Arce, A. Schaadt, H.J. Bart, Extraction with spinodal decomposition-experiment and simulation, Chem. Eng. Technol. 29 (4) (2006) 487–494.
[20] P. Poesio, A.M. Lezzi, G.P. Beretta, Evidence of convective heat transfer enhancement induced by spinodal decomposition, Phys. Rev. E 75 (2007) 066306/1–066306/9.
[21] H. Husen, Darstellung des warmeuberganges in rohren durch verallgemeinerte potenzbeziehungen, VDI Z., 4 (1943) 91.
[22] S.W. Churchill, H.H.S. Chu, Correlating equations for laminar and turbulent free convection from a horizontal cylinder, Int. J. Heat Mass Transfer 18 (1975) 1049–1053.
[23] A. Ullmann, N. Brauner, The prediction of flow pattern maps in mini channels, Multiphase Sci. Technol. 19 (1) (2007) 49–73.
[24] G. Rabinski, D. Thomas, Dynamic digital image analysis: emerging technology for particle characterization, Internal Water Association (2003).
[25] N. Vladimirova, A. Malagoli, R. Mauri, Two dimensional model of phase segregation in liquid binary mixtures with an initial concentration gradient, Chem. Eng. Sci. 55 (2000) 6109–6118.
[26] G. Santonicola, R. Mauri, R. Shinnar, Phase separation of initially non-homogeneous liquid mixtures, Ind. Eng. Chem. Res. 40 (2001) 2004–2010.
[27] J.M. Sorensen, W. Arlt, Liquid–Liquid Equilibrium Data Collection: Ternary Systems, Chemistry Data Series, vol. v, part 2, Dechema, 1980, pp. 333–339.
[28] A. Arce, L. Alonso, I. Vidal, Liquid–liquid equilibria of the systems ethyl acetate + ethanol + water, butyl acetate + ethanol + water, and ethyl acetate + butyl acetate + water, J. Chem. Eng. Jpn. 32 (4) (1999) 440–444.
[29] H.M. Lin, C.E. Yeh, G. B Hong, M.J. Lee, Enhancement of liquid phase splitting of water + ethanol + ethyl acetate mixtures in the presence of a hydrophilic agent or an electrolyte substance, Fluid Phase Equilibr. 237 (1–2) (2005) 21–30.
[30] S.C. McCutcheon, J.L. Martin, T.O. Barnwell, Handbook of Hydrology, McGraw-Hill, New York, NY, 1993. p. 113.
[31] K.N. Marsh, Material for the Realization of Physicochemical Properties, Blackwell, Oxford, 1987.
[32] C.A. Nieto de Castro, S.F. Li, A. Nagashima, R.D. Trengove, W.A. Wakeham, Standard reference data for the thermal conductivity of liquids, J. Phys. Chem. Ref. Data 15 (1986) 1073–1085.
[33] R. Belda, J.V. Herraez, O. Diez, Rheological study and thermodynamic analysis of the binary system (water/ethanol): influence of concentration, Phys. Chem. Liq. 42 (5) (2004) 467–479.
[34] H. Djojoputro, S. Ismadji, Density and viscosity correlation for several common fragrance and flavor esters, J. Chem. Eng. Data 50 (2) (2005) 727–731.
[35] M. Zabransky, V. Hynek, J. Finkeova-Hastabova, F. Vesely, Heat capacity of six liquid esters as a function of temperature, Collect. Czech. Chem. Commun. 52 (1987) 251–257.
[36] ESDU, Engineering Science Data Unit, <www.esdu.com>.
[37] A. Valtz, M. Teodorescu, I. Wichterle, D. Richon, Liquid densities and excess molar volumes for water + diethylene glycolamine, and water, methanol, ethanol, 1-propanol + triethylene glycol binary systems at atmospheric pressure and temperatures in the range of 283.15–363.15 K, Fluid Phase Equilibr. 215 (2004) 129–142.
[38] F.E. Blacet, P.A. Leighton, E.P. Bartlett, The specific heats of five pure organic liquids and of ethyl alcohol–water mixtures, J. Phys. Chem. 35 (7) (1931) 1935–1943.
[39] Q.F. Lei, S.R. Lin, D.Y. Ni, A new correlation of thermal conductivities of liquids, Chem. Eng. Sci. 52 (1997) 1243–1251.
[40] R.M. Pires, H.F. Costa, A.G.M. Ferreira, I.M.A. Fonseca, Viscosity and density of water + ethyl acetate + ethanol mixtures at 298.15 and 318.15 K and atmospheric pressure, J. Chem. Eng. Data 52 (4) (2007) 1240–1245.